Energy Landscape of the Prion Protein Helix H1 Probed by Metadynamics and NMR

Carlo Camilloni,[1] Daniel Schaal,[2] Kristian Schweimer,[2] Stephan Schwarzinger,[2,*], Alfonso De Simone[3,*]

[1]*Department of Chemistry, University of Cambridge, Lensfield Road, CB2 1EW Cambridge, United Kingdom.* [2]*Lehrstuhl Biopolymere and Research Center for Bio-Macromolecules, Universität Bayreuth, Universitätsstrasse 30, 95447 Bayreuth, Germany.*[3]*Division of Molecular Biosciences, Imperial College London, South Kensington, London SW7 2AZ, UK*
**correspondence to: stephan.schwarzinger@uni-bayreuth.de; a.de-simon@imperial.ac.uk;*

Supplementary Materials and Metods

Parallel Tempering Metadynamics Sampling

The conformational sampling of PrP_H1 has been performed by using a combination of Parallel Tempering and Metadynamics (PT-MetaD) (1-4) as previously adopted to sample FES of a β-hairpin (1). A detailed description of the employed probability of exchange is reported elsewhere (1). PT-MetaD have been carried out by employing 50 replicas ranging from 283 K to 471 K (283.0 K, 286.0 K, 289.0 K, 292.0 K, 295.0 K, 298.1 K, 301.2 K, 304.3 K, 307.5 K, 310.7 K, 313.9 K, 317.2 K, 320.5 K, 323.8 K, 327.2 K, 330.6 K, 334.1 K, 337.6 K, 341.1 K, 344.7 K, 348.3 K, 351.9 K, 355.6 K, 359.3 K, 363.1 K, 366.9 K, 370.7 K, 374.6 K, 378.5 K, 382.5 K, 386.5 K, 390.5 K, 394.6 K, 398.7 K, 402.9 K, 407.1 K, 411.4 K, 415.7 K, 420.1 K, 424.5 K, 429.0 K, 433.5 K, 438.0 K, 442.6 K, 447.2 K, 451.9 K, 456.6 K, 461.4 K, 466.2 K and 471.1 K) and extended for 48 ns. The reconstructed FES was averaged over the converged part of the simulation.

We employed the direct formulation of metadynamics (5) and performed the calculations by using the PLUMED (6) plug-in applied to GROMACS (7). Metadynamics simulations are performed by means of a set of functions of the system coordinates *s(x)*, namely the collective variables (CVs). These are normally selected in order to describe the conformational features of the system. Not only the CVs should account for relevant species of the ensemble, but should also include the "slow" variables along which the sampling performs the principal exploration of the configurational phase space. The phase space exploration is then guided along the CVs by the free energy of the system plus a history-dependent potential having the functional form of a sum of Gaussians that are functions of the CVs and the time *t*:

$$V_m(\vec{s},t) = w_m \sum_{t_k<t} \exp\left(-\sum_i \frac{(s_i - s_i(X_m(t_k)))^2}{2\sigma_i^2} \right) \quad (1)$$

where w is the weight and σ is the width of the Gaussians along the i-th CVs. We employed the number of hydrogen bonds (N_H) between residues i and $i+4$, defined as sum of step functions of the distance between backbone hydrogen and oxygen atoms:

$$N_H = \sum_{i=1}^{11} \frac{1-(r_{i,i+4}/d_0)^n}{1-(r_{i,i+4}/d_0)^m} \quad (2)$$

where n=6, m=12 and d_0=0.25 nm, and the radius of gyration (R_g) measured over the C^α atoms. These variables were shown to be effective for studying the folding of an alpha helix (8). It is worth nothing that the variable N_H yields to a continuous function (a fundamental requisite for a CV), which implies that a given conformation can be featured by a non-integer number of N_H. The parameters employed for the hills were: w = 0.2 kJ/mol, σ_{N_H} = 0.06, σ_{Rg}= 0.03 nm and interval between the deposition of two Gaussians was τ_G = 1 ps.

NOE-based structure determination of Helix 1 Conformers

The NMR NOESY spectra of the prion protein helix 1 (PrP-H1) peptide show numerous inter-residual NOE signals, which could in principle be used for structure calculation using traditional distance restraints (10). We here show, however, that despite the possibility to calculate helical structures these are not in agreement with the intensities observed in the NOESY spectra due to the high flexibility of the peptide and the subsequent conformational averaging (10, 11). Moreover, the resulting well-converging ensemble of structures does not reflect the structural properties, i.e. the helix content and conformational heterogeneity, that may be expected from chemical shift and circular dichroism data (9). We show by calculation of structural ensembles based on NMR distance and dihedral restraints that the resulting ensembles do not adequately represent the ongoing fast exchange between conformations.

For structure calculation the same NMR-data set used to obtain the assignments were employed. Structure calculation was carried out using the XPLOR-NIH package (12, 13). NOE signal intensities were picked in a 300 ms NOESY spectrum acquired at 800 MHz after verifying that the NOE build-up is in agreement with the initial rate approximation by inspecting the signal intensities from spectra with mixing times of 100, 200, and 300 ms, respectively (11). Signal intensities were referenced relative to the intensity of the intra-residual H^N-H^α signal, which shows only minimal variations of the distance of these two nuclei in the different secondary structure elements (α-helix: 2.8 Å; β-strand: 3.0 Å) and therefore was set to 3.0 Å as an upper distance boundary. It should be mentioned that – although in a flexible peptide conformations with shorter H^N-H^α signal may be explored – this rather conservative choice is reasonable in view of the fact that significant populations of conformers deviating from the above mentioned distances are absent in the ensemble determined by PT-MetaD (i.e. as shown in figure S4 D). Hence, signals of equal or stronger intensities were accordingly assigned upper distance limits of 3 Å. The remaining signals were categorized following a r^{-6}-dependece and assigned upper distance limits of 3.5 Å, 4.5 Å, and 5.5 Å, respectively. Side chain signals that were not assigned stereospecifically were treated as ambiguous restraints. Secondary chemical shifts were converted into dihedral restraints with the program TALOS and applied to residues exhibiting the strongest $^{13}C^\alpha$-secondary shifts, i.e. residues 148 - 152 and residue 154 (14). The best 20 out of 100 calculated structures were used for further analysis. Ramachandran statistics were evaluated by PROCHECK (15).

The NOE-based NMR structural ensemble

The technological and methodological advancements of the recent years allow the collection of very high quality NMR data sets on a routine basis. Even for rather flexile systems, NOE-patterns can be found that are caused by conformers corresponding to defined secondary structure elements making it attempting to derive at least "preferred conformers". Here, 800 MHz-NOESY spectra with a very high signal-to-noise ratio were evaluated in order to assess whether NOE-signals arising from conformers corresponding to secondary structure elements could be identified. Of note, it was not possible to identify NOE cross peaks patterns that could not be explained by helical conformations. This is interesting as this observation largely excludes the presence of significant populations of conformations with β-sheet and turn-like structures. However, close inspection of the NOE-patterns and intensities reveals that, e.g., many of the $H^{\alpha,i}$-$H^{N,i+3}$ – which have a distance of 3.5 Å in an α-helix – are too weak or even missing. In contrast, essentially all $H^{\alpha,i}$-$H^{N,i+1}$ (α-helix: 3.5 Å; β-strand: 2.2 Å) cross peaks exhibit intensities stronger than intra-residual $H^{\alpha,i}$-$H^{N,i}$ signal (Figure S4), which is used as an internal reference. Hence, the NOE-intensities provide clear evidence for structural heterogeneity. However, because structure calculation is driven in a manner that requires all restraints to be fulfilled simultaneously, the resulting structural ensembles will be over-restrained and will therefore no reflect the proper distribution of secondary structure elements in the ensemble.

In fact, the ensemble of structures calculated on the basis of a total of 210 distance restraints (88 intra-residual; 122 inter-residual, 75 of which are consecutive restraints and 21 of which are i,i+2 while 26 of these are i,i+3 and i,i+4 restraints) exhibits an α-helical core (R148-E152) flanked a distorted helix extending to residue Y145 at the amino-terminus and to residue N154 at the carboxy-terminus, respectively (Figure S5-A). The α-helical core, which coincides with the residues showing the highest $^{13}C^{\alpha}$ secondary chemical shifts, also exhibits very well ordered side chains. The helical region in this structural ensemble, consisting of the α-helical core as well as the distorted helical termini, extends from residue 145 to 154, which sums up to a helix-content higher than found by CD and NMR-secondary chemical shift. In fact, this ensemble most closely resembles the basin b3 of the PT-MetaD simulations, which however is the lowest populated minimum in the free energy surface. The too large helix content is a consequence of the way the structure calculation is conducted, where all restraints are fulfilled simultaneously. Assessment of the quality of the structure indeed shows violations of the NOE restraints and a non-optimal distribution in the *phi-psi* space. The violations, although not being very large, mostly relate to those distances that were found to be too short for a α-helical conformation. These are the only indicators for incompatibility of the calculated structure with the experimental data. It shall be pointed out that proper referencing and classification of the NOE intensities is mandatory to be able to identify these indicators of incompatibility.

In the following we briefly demonstrate that variations of the restraints for the structure does not significantly reduce the amount of helical structure in the peptide. First, 12 dihedral restraints derived from TALOS were applied in addition to the NOE distance restraints. Not unexpectedly, the α-helical core even extends, while the termini display an enhanced conformational flexibility (Figure S5-B). The additional torsion angle restraints result in a slightly better distribution of the main chain torsion angels in the Ramachandran plot, but result in even worse NOE violations. Inclusion of the additional restraints in the particular case increases over-restraining and is not suited to improve a proper structural representation of the conformational ensemble.

Next, intra-residual distance restraints were removed to evaluate their effect on the structure. In the case of stably folded proteins where the structure is typically determined by a sufficient

number of inter-residual NOEs, removal of the intra-residual NOEs normally does not disturb the structure obtained. In the present case removing the intra-residual overall increases flexibility in the ensemble, while leaving the helix content essentially unchanged (Figure S5-C). In comparison to the structures obtained with all distance restraints a similar distribution in the Ramachandran space was obtained, while the number of NOE-violations are was decreased. This result can be interpreted as incompatibility of the conformations found in the side-chains with those of the main chain, which can be explained by conformational exchange.

Finally, a calculation was carried out with a set of NOE-restraints that were categorized less strictly. In particular, only three classes of NOEs were used corresponding to distances of 3.5 Å, 4.5 Å, and 5.5 Å, respectively. The resulting structural ensemble comprises a single, well defined α-helix with more than 90 % of the back bone dihedrals populating the most preferred regions in the Ramachandran plot (Figure S5-D). Loosening of the distance classification, i.e. deviating from the r^{-6} distance dependence of NOE signal intensities, does not result in NOE-violations any more. According to these standards, the structure obtained would be of high quality. In fact, this ensemble is least suited to represent the conformational behavior of the PrP-H1 peptide.

The examples presented underline the problem with conventional structure calculation based on distance and torsion angle restraints derived from systems exhibiting conformational exchange and emphasizes the strength of PT-MetaD combined with experimental data to properly describe the FES. Due to the requirement that the restraints have to be fulfilled simultaneously, the resulting conformation will always be over-restrained and does not provide a proper representation of the conformational ensemble. In fact, even using subsets of restraints does not yield satisfying results. In particular, the removal of the distance restraints that determine the helical conformations in the present example result in a conformational ensemble of exclusively extended structures, determined by the strong consecutive distance restraints (data not shown). Again, the resulting ensemble of structures is not suited to reflect the conformational heterogeneity of the PrP-H1 peptide. It rather is more representative of a fraction of entirely unfolded ensemble. Hence, even combination of the helical conformers obtained and the extended conformers cannot describe the FES of the PrP-H1 peptide. Overall, it should be mentioned that selection of a sub-state of restraints from a system exhibiting fast conformational exchange should be discouraged, as it is not known which restraints apply for a given conformer of the ensemble. Also, it should be emphasized (i) that NOE intensities always have to be accurately calibrated, (ii) that NOE built-up curves should be analyzed and (iii) that close attention has to be paid to intensity of NOE cross peaks that are incompatible with the peak patterns anticipated for a given secondary structure element, as this indicates structural heterogeneity in the sample.

Back calculation of NOE intensities from the structural ensembles

NOEs were calculated by analyzing the PT-MetaD ensemble. As PT-MetaD does not allow to extract rotational correlation times, iterative relaxation matrix analysis cannot be performed. As a result, NOE intensities are assumed to follow an r^{-6} dependence of the reweighted distances of the ensemble. For each pair of hydrogen atoms A and B, reweighted distances $\langle r_{AB} \rangle$ or $\langle r^{-6}_{AB} \rangle$ were calculated by using the following integrations:

$$< r_{AB} >= \frac{\int r_{AB} \cdot \exp\left(-\frac{F(r_{AB})}{2.35} \right) dr}{\int \exp\left(-\frac{F(r_{AB})}{2.35} \right) dr} \qquad (3)$$

$$< r_{AB}^{-6} >= \left(\frac{\int r_{AB}^{-6} \cdot \exp\left(-\frac{F(r_{AB}^{-6})}{2.35} \right) dr}{\int \exp\left(-\frac{F(r_{AB}^{-6})}{2.35} \right) dr} \right)^{-1/6} \quad (4)$$

where F(r_{AB}) and F(r^{-6}_{AB}) are the projections of the free energy onto reaction coordinates r_{AB} and r^{-6}_{AB}, respectively, and are calculated with the reweighting method proposed by Parrinello and coworkers (16, 17) and here adopted to reweight also chemical shifts. Distances involving equivalent hydrogen atoms (e.g. HB2 and HB3) were averaged.
$<r^{-6}_{AB}>$ resulted in very good agreement with experimental data (Table S2) by satisfying 90.6% of the NOEs in the fingerprint region of the NOESY spectrum (i.e. involving HN and H^{α} atoms). The agreement raises to 96.2% with a tolerance of 0.5 Å and 98.1% with a tolerance of 1 Å. Very good agreement is also found when other hydrogen atoms are included in the statistics (Table S2).
In the previous section we pointed out how measured NOESY peak intensities are not compatible with a fully helical structure and suggest structural heterogeneity (Figure S4 B). Remarkably, distributions of reweighted distances $<r_{AB}>$ (eq. 3) from the PT-MetaD ensemble provide a description of the ensemble's structural fluctuations underlying the observed intensities of the measured NOESY signals. This is here showed by analyzing the distributions of $<r_{AB}>$ corresponding to the pairs of atoms associated with the peaks shown in Figure S4 B. The reweighted intra-residual H^{α}-H^{N} distance distribution (Figure S4 D) for N153 shows a single population centered at 2.9 Å, which would correspond to an intense cross peak in the NOESY spectrum, while the distribution of 152(H^{α})-153(H^{N}) distances presents two peaks: one corresponding to alpha-helical structures (3.4 Å) and the other to extended/random-coil conformations (2.2 Å). This double distribution is in line with an intense cross peak for 152(H^{α})-153(H^{N}) as observed in the NOESY spectrum. On the other hand, a fully helical structure would have provided a less intense peak for 152(H^{α})-153(H^{N}) compared to the intra-residue peak (e.g. see the case of yeast ubiquitin in Figure S4 C). In fact, the same behavior is found for the structural ensemble calculated by conventional methods (Figure S5 A), where the intensity of the back-calculated sequential H^{α}-H^{N} NOEs is smaller than the intra-residual H^{α}-H^{N} (on average 46 % *vs*. 144 % in the experimental data), thus providing direct evidence for over-restraining in the NOE-based structure calculation that results into an overestimations of the helical fraction in the resulting structural ensemble. The back calculated distances for 150(H^{α})-153(H^{N}) in the PT-MetaD ensemble are broadly distributed with either distances that are typical of alpha-helix conformations (i.e. 3.5 Å) and larger distances arising from extended/random-coil structures. This distribution is compatible with a weak cross peak in the NOESY spectrum. Finally, 149(H^{α})-153(H^{N}) is associated with a significantly broad distribution (Figure S4 D) which is in line with a weak NOESY peak. Overall, the reweighted distances from the PT-MetaD ensemble are able to provide a structural description of the intensities of the NOESY with a better agreement then a fully helical structure as obtained by conventional NOE-based methods.

References

1. Bussi, G., F. L. Gervasio, A. Laio, and M. Parrinello. 2006. Free-energy landscape for beta hairpin folding from combined parallel tempering and metadynamics. J Am Chem Soc 128:13435-13441.
2. Bussi, G., A. Laio, and M. Parrinello. 2006. Equilibrium free energies from nonequilibrium metadynamics. Phys Rev Lett 96:090601.
3. Hansmann, U. H. E. 1997. Parallel tempering algorithm for conformational studies of biological molecules. Chem Phys Lett 281:140-150.
4. Laio, A., and M. Parrinello. 2002. Escaping free-energy minima. Proc Natl Acad Sci U S A 99:12562-12566.
5. Laio, A., and F. L. Gervasio. 2008. Metadynamics: a method to simulate rare events and reconstruct the free energy in biophysics, chemistry and material science. Rep Prog Phys 71:-.
6. Bonomi, M., D. Branduardi, G. Bussi, C. Camilloni, D. Provasi, P. Ralteri, D. Donadio, F. Marinelli, F. Pletrucci, R. A. Broglia, and M. Parrinello. 2009. PLUMED: A portable plugin for free-energy calculations with molecular dynamics. Comp. Phys. Comm. 180:1961-1972.
7. Hess, B., C. Kutzner, D. van der Spoel, and E. Lindahl. 2008. GROMACS 4: Algorithms for highly efficient, load-balanced, and scalable molecular simulation. J Chem Theory Comput 4:435-447.
8. Camilloni, C., D. Provasi, G. Tiana, and R. A. Broglia. 2008. Exploring the protein G helix free-energy surface by solute tempering metadynamics. Proteins 71:1647-1654.
9. Ziegler, J., H. Sticht, U. C. Marx, W. Muller, P. Rosch, and S. Schwarzinger. 2003. CD and NMR studies of prion protein (PrP) helix 1. Novel implications for its role in the PrPC-->PrPSc conversion process. J Biol Chem 278:50175-50181.
10. Wüthrich. 1986. NMR of Proteins and Nucleic Acids, John Wiley & Sons.
11. Neuhaus, D., and M. Williamson. 1989. The Nuclear Overhauser Effect in Structural and Conformational Analysis, John Wiley & Sons.
12. Schwieters, C. D., J. J. Kuszewski, and G. M. Clore. 2006. Using Xplor-NIH for NMR molecular structure determination. Prog Nucl Mag Res Sp 48:47-62.
13. Schwieters, C. D., J. J. Kuszewski, N. Tjandra, and G. M. Clore. 2003. The Xplor-NIH NMR molecular structure determination package. J Magn Reson 160:65-73.
14. Cornilescu, G., F. Delaglio, and A. Bax. 1999. Protein backbone angle restraints from searching a database for chemical shift and sequence homology. Journal of Biomolecular Nmr 13:289-302.
15. Laskowski, R. A., J. A. C. Rullmann, M. W. MacArthur, R. Kaptein, and J. M. Thornton. 1996. AQUA and PROCHECK-NMR: Programs for checking the quality of protein structures solved by NMR. Journal of Biomolecular Nmr 8:477-486.

16. Barducci, A., M. Bonomi, and M. Parrinello. 2010. Linking well-tempered metadynamics simulations with experiments. Biophys J 98:L44-46.
17. Bonomi, M., A. Barducci, and M. Parrinello. 2009. Reconstructing the equilibrium Boltzmann distribution from well-tempered metadynamics. J Comput Chem 30:1615-1621.
18. Petrucci, F., and A. Laio. 2009. A Collective Variable for the Efficient Exploration of Protein Beta-Sheet Structures: Application to SH3 and GB1. J Chem Theory Comput 5:2197-2201.
19. De Simone, A., A. Zagari, and P. Derreumaux. 2007. Structural and hydration properties of the partially unfolded states of the prion protein. Biophys J 93:1284-1292.
20. Schwarzinger, S., A. H. Horn, J. Ziegler, and H. Sticht. 2006. Rare large scale subdomain motions in prion protein can initiate aggregation. J Biomol Struct Dyn 23:581-590.

Table S1. Structural Determination by NOEs and Dihedral Restraints

PrP-H1 structure calculation (20 lowest energy structures)		Set			
		NOE (3.0/3.5/4.5/5.5 Å)	NOE (3.0/3.5/4.5/5.5 Å) + TALOS	inter-residual NOEs (3/3.5/4.5/5.5 Å)	"loosened" NOEs (3.5/4.5/5.5 Å)
Experimental restraints					
NOEs		210	210	122	210
Dihedrals		0	12	0	0
NOE violations (Å)					
	>0.3	1.9 ± 1.1	3.8 ± 1.3	1.0 ± 0.9	0
	>0.1	20.5 ± 2.0	20.5 ± 1.9	12.6 ± 1.7	0.10
	NOE RMSD	0.076 ± 0.002	0.071 ± 0.001	0.077 ± 0.003	0.079 ± 0.002
Back-bone RMSD to mean structure (Å)		1.01	1.29	1.17	0.94
Average number of H-Bonds		1.3	2.2	1.1	3.5
Ramachandran analysis (%)					
Most favoured		67.3	66.9	70.0	95.0
Additionally allowed		28.5	30.8	26.9	4.2
Generously allowed		4.2	2.3	2.3	0.8
Disallowed		0.0	0.0	0.8	0.0

Table S2. Comparison of experimental and back-calculated NOEs. The table reports the percentage of $\langle r^{-6}_{AB} \rangle$ satisfying the NOEs' upper bounds. The statistics are performed by using a tolerance of 0.0, 0.5, 1.0 and 2.0 Å and have been produced on different sets of atoms.

	Tol = 0.0Å	**Tol = 0.5Å**	**Tol = 1.0Å**	**Tol = 2.0Å**
H^N, H^α	90.6%	96.2%	98.1%	100.0%
H^N, H^α, H^β	73.6%	83.5%	88.4%	91.7%
All	64.0%	75.9%	83.3%	89.7%

Supplementary Figures

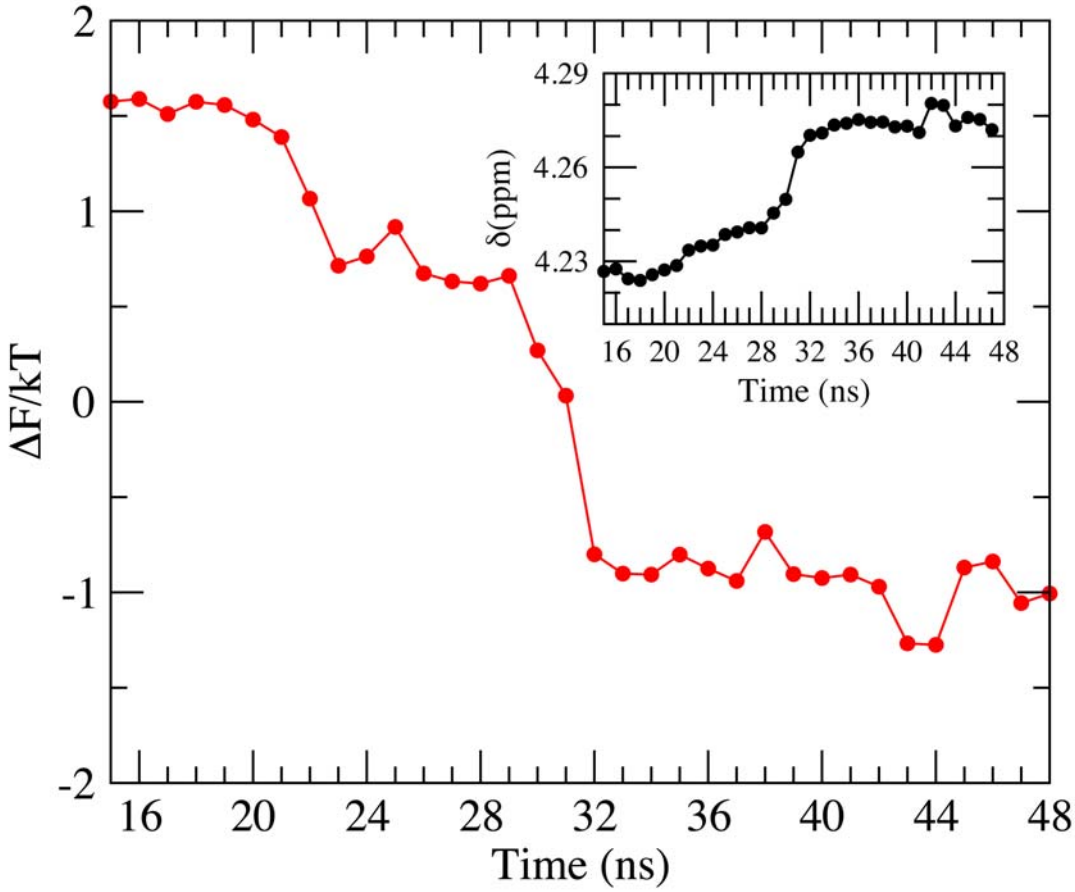

Figure S1. PT-MetaD convergence. In the main plot it is shown the difference in the energy values of two principal regions of the FES as a function of the time. The plot reports the free-energy difference between the regions with Hbonds ("*i, i+4"*) <= 4 and Hbonds ("*i, i+4*") > 4 as a function of time. This free-energy difference reaches a steady state after 32 ns of simulation. In the top-right inset is showed the convergence of the back-calculated chemical shift of the $^{1}H^{\alpha}$ atom of residue Ala143. The two plots converge simultaneously.

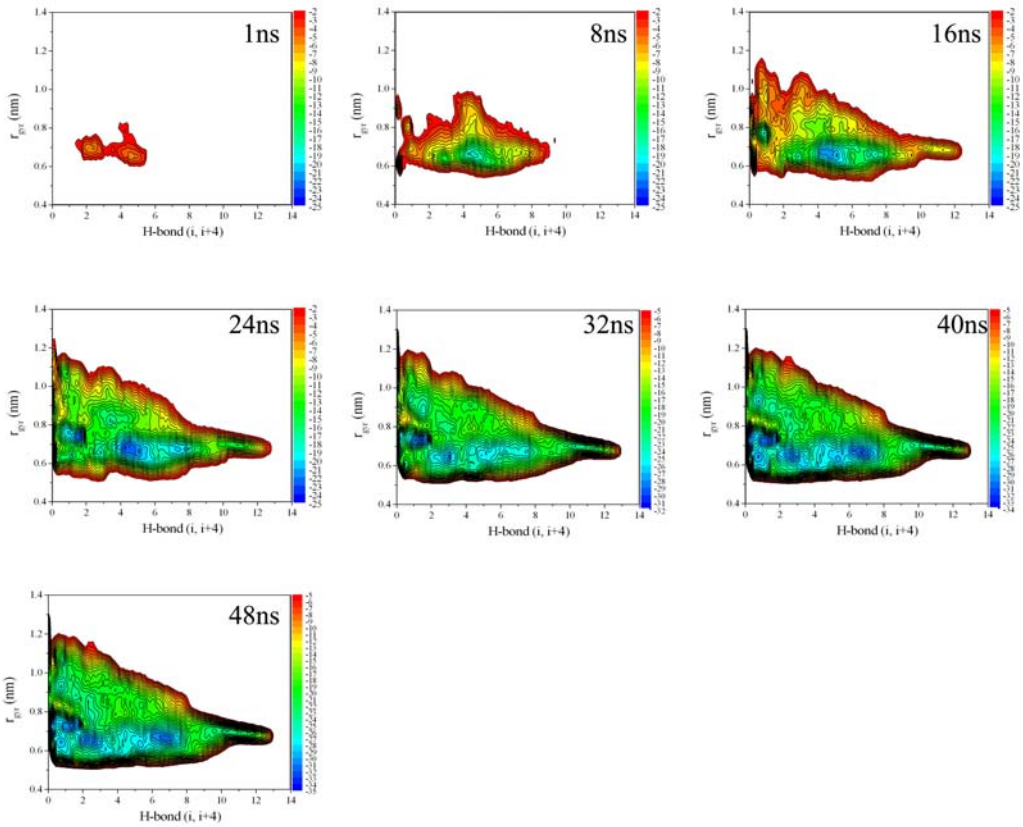

Figure S2. Time evolution of the PrP-H1 FES sampled by PT-MetaD

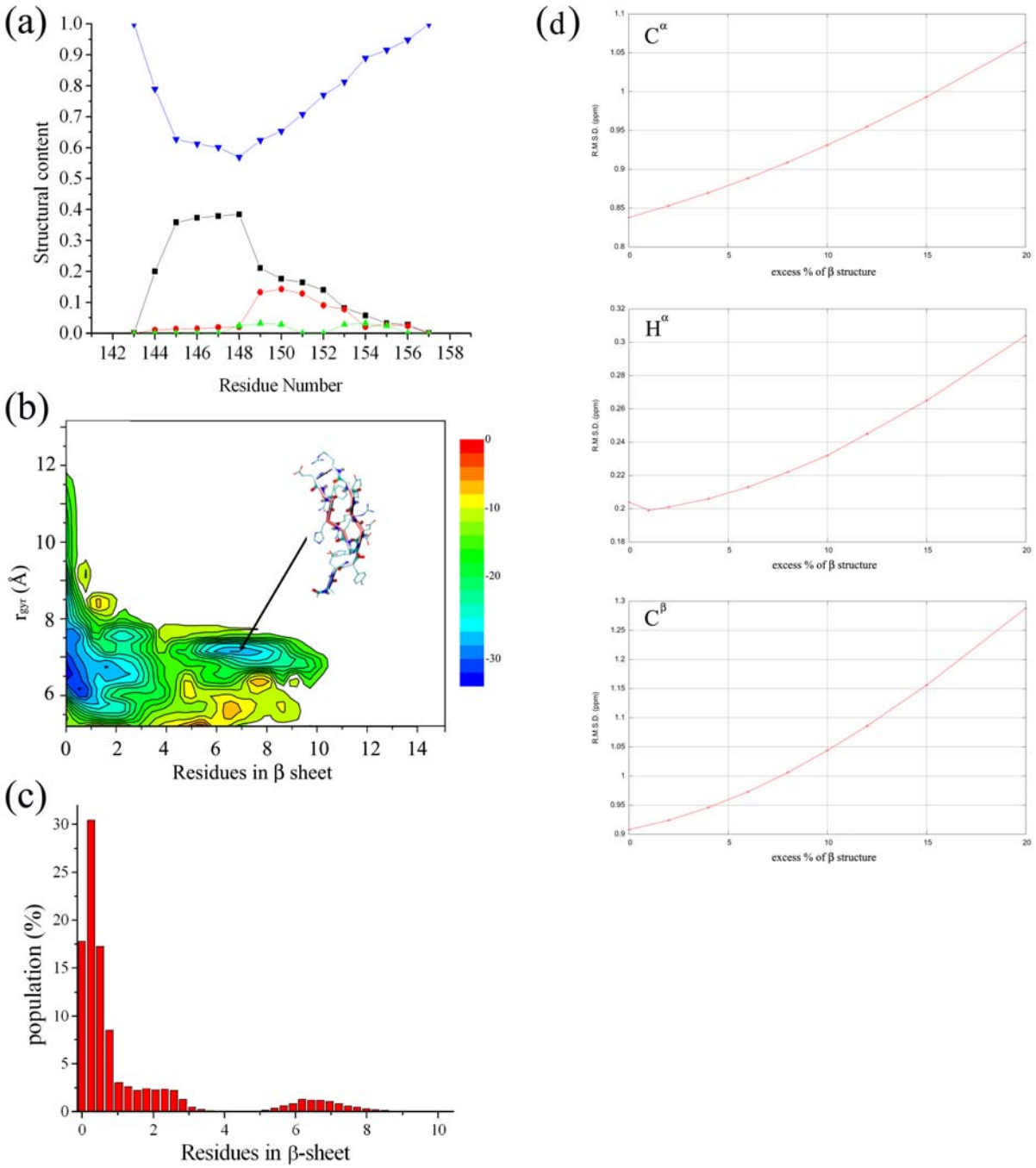

Figure S3. Secondary structure content in the PT-MetaD ensemble. A) Reweighted Secondary structure profiles. Alpha helix, 3_{10} helix, β-sheet and random coil profiles are shown in black, red, green and blue, respectively. B) Re-projected FES on a β-sheet coordinate (i.e. as defined in (18)). The major portion of the sampling is located at the minimum presenting a number of residues in β-sheet lower than 2.0. An additional basin is highlighted for having a number of residues in β-sheet conformation ranging from 5 to 8. This basin hosts mainly β-hairpin conformations. A representative structure is drawn. C) Reweighted populations along the β-sheet coordinate. The total area of the β-sheet conformation is 9%. As in this basin the total amount of residues being in β-sheet conformation ranges from 5 to 8, the weight on the whole sequence is 3.5% of β-sheet content. D) Estimation of the errors on the β-sheet population by chemical shifts. The three plots report the RMSD values between experimental and calculated chemical shifts as a function of additional population of β-sheet conformation as sampled in the present PT-MetaD sampling (panel B). From these plots, the best agreements are found at 0%, 0% and 1% of additional population of β-sheet population for C^{α} and C^{β} and H^{α}, respectively.

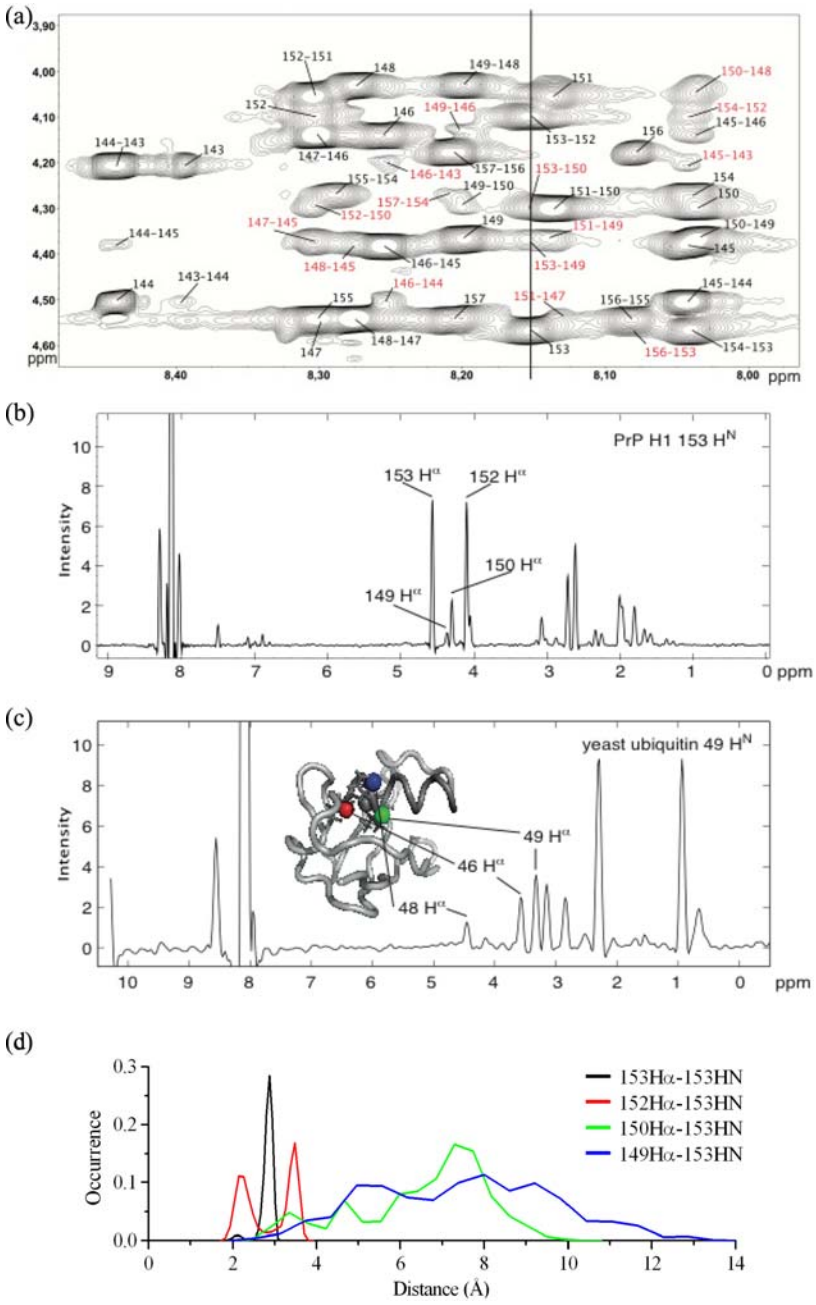

Figure S4. A) H^N/H^α-section of the 800 MHz NOESY spectrum of PrP-H1. Intra-residual and consecutive cross peaks are labeled black, with the H^N-frequency mentioned in the first position. Cross peaks corresponding to helical conformations are labelled in red. The vertical line marks the position of the trace shown in panel B. B) Trace along the H^N-frequency of N153 of the PrP-H1 NOESY spectrum. In a α-helix the distances between the H^N and the H^α of the preceding residue and the i-3 residue should be equivalent (~3.5 Å). However, it can clearly be seen that the intensity of the cross peak 150(H^α)-153(H^N) is much smaller that the intensity of the 152(H^α)-153(H^N) cross peak. On the other hand, in a β-sheet the distance between H^N and the intra-residual H^α is ~3.0 Å, while the distance between the H^N and the H^α of the preceding residue is ~2.2 Å. Hence, the corresponding cross peak for the consecutive NOE should be of much higher intensity than the intra-residual cross peak for β-sheet conformations, which is also not the case here. The observed discrepancies in NOE intensities can be explained by fast exchange between conformations on the NMR time-scale. C) Trace along the H^N-frequency of V49, which residues in the α-helix of yeast ubiquitin and which shall serve as an example for NOE intensities, as they are typically found in helices. The H^N of V49 is depicted as a gray sphere in the insert, V49-H^α is shown in green. It can clearly be seen that the cross peak with the i-3-spaced H^α of I46 (red sphere) is even stronger than cross peak with the preceding H^α of N48 (blue sphere). D) Reweighted distance distributions in the metadynamics ensemble of PrP-H1. Color codes are black, red, green and blue for 153(H^α)-153(H^N), 152(H^α)-153(H^N), 150(H^α)-153(H^N) and 149(H^α)-153(H^N), respectively. The atom pairs correspond to the cross peaks as shown in panel B.

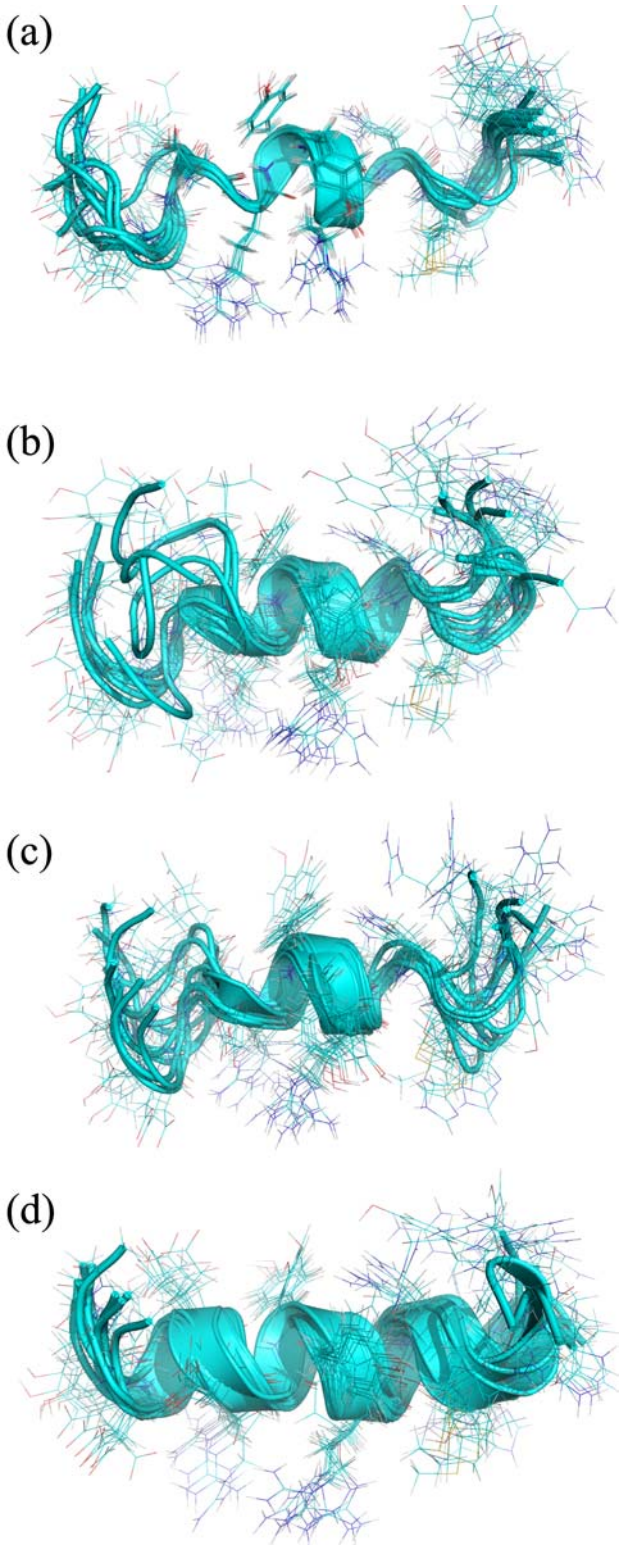

Figure S5 Conformational ensembles calculated on the basis of NMR distance and dihedral restraints: A) 210 NOE restraints, B) 210 NOE restraints and 12 dihedral restraints, C) 122 inter-residual NOEs, D) 210 “loose” NOE restraints.

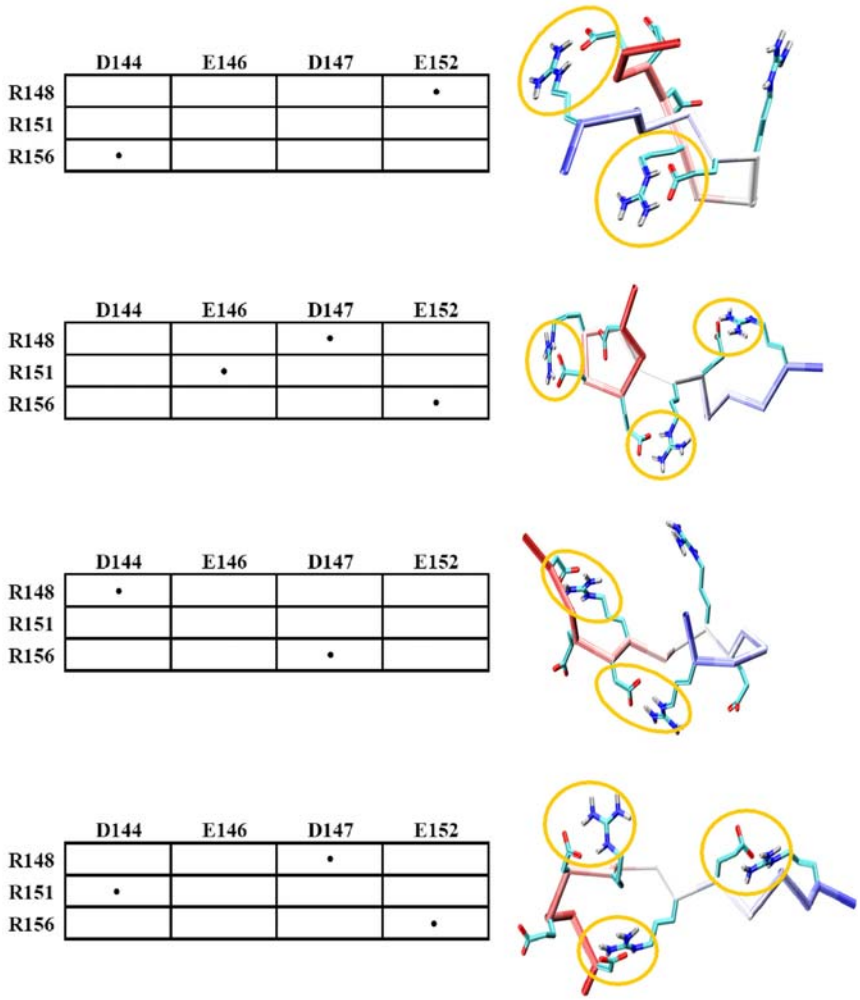

Figure S6. Examples of salt bridges configurations for RC conformations. Left tables report the residues engaged in the salt bridge in the specific configuration. Orange circles on the conformations on the right indicate salt bridges. Right panels draw the PrP-H1 peptide by means of C^{α}-trace. Side chains of charged residues are also drawn explicitly.

	D144	E146	D147	E152
R148	•			
R151			•	
R156				•

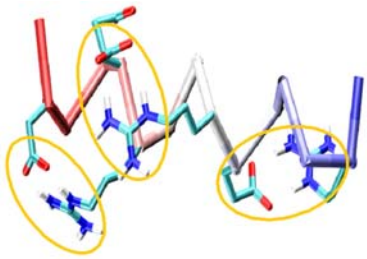

	D144	E146	D147	E152
R148	•			
R151			•	
R156				

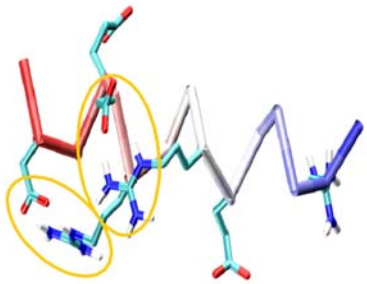

Figure S7. Principal salt bridges configurations of the helical conformation. Left tables report the residues engaged in the salt bridge in the specific configuration. Orange circles on the conformations on the right indicate salt bridges. Right panels draw the PrP-H1 peptide by means of C^{α}-trace. Side chains of charged residues are also drawn explicitly.

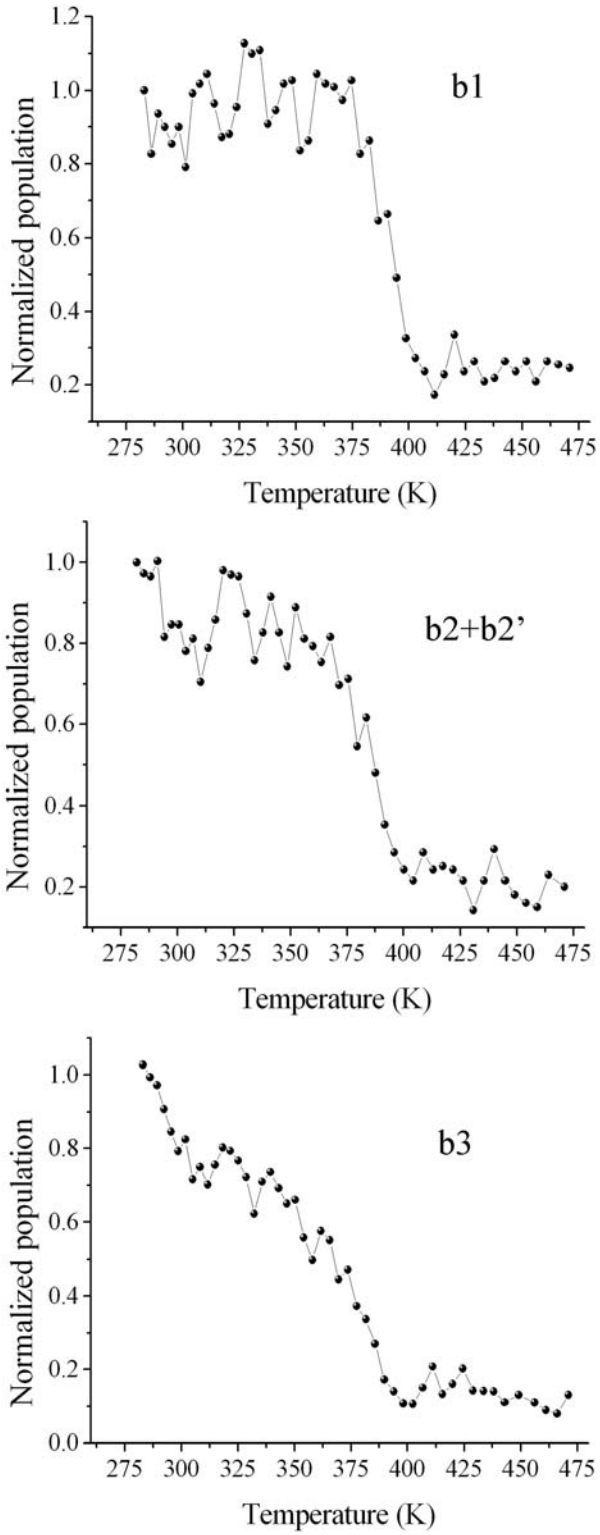

Figure S8. Temperature dependence of the normalized populations for helical basins of the FES.

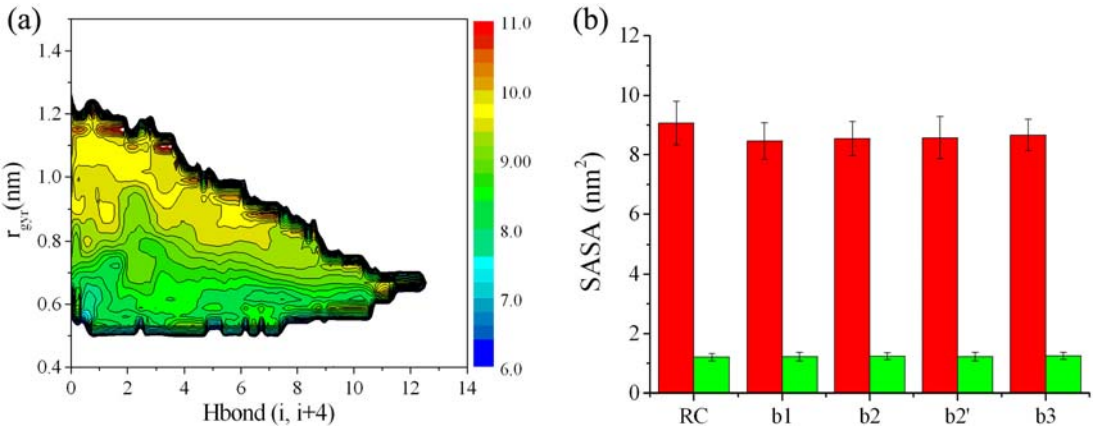

Figure S9. Hydrophobic exposed surface. (A) Average hydrophobic SASA as a function of the CVs. (B) Hydrophobic (red) and aromatic (green) SASAs for each relevant free-energy basin.

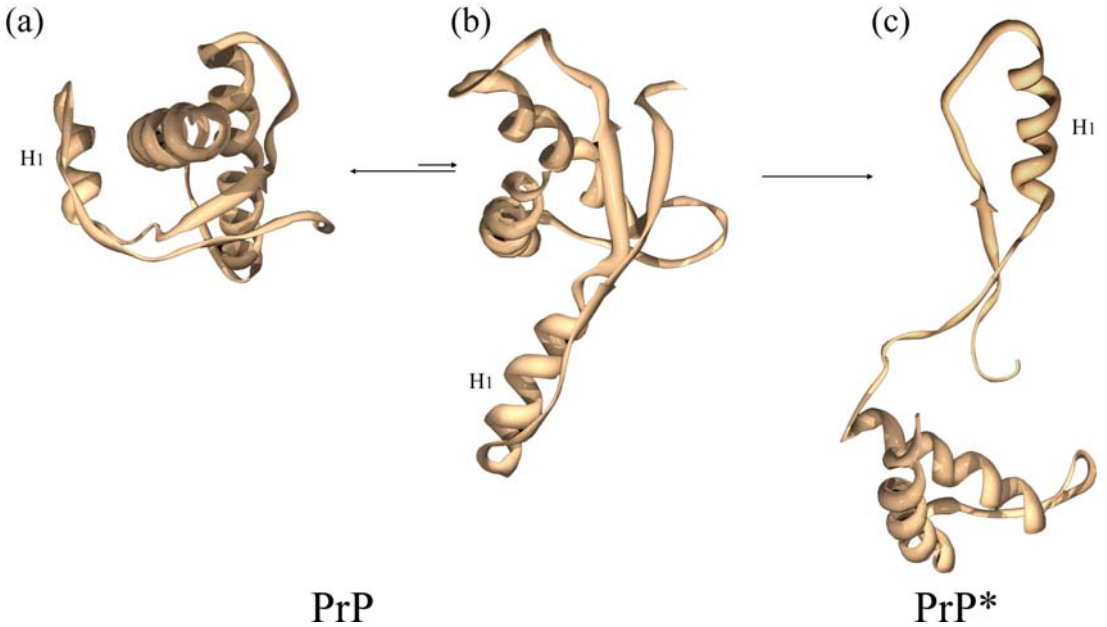

Figure S10. Schematic model of the early stages of PrP misfolding. A) PrP native structure. B) Structural intermediate promoted by a native breathing motion in which PrP-H1 detaches from the native interface. C) Non native fluctuations on the pathway of the large breathing motions can lead the protein to explore dangerous activated conformations for self-assembly into amyloids. In this model PrP* is featured by a complete detachment of the subdomains S1-H1-S2 and H2-H3, which is consistent with many experimental and theoretical studies (19, 20).

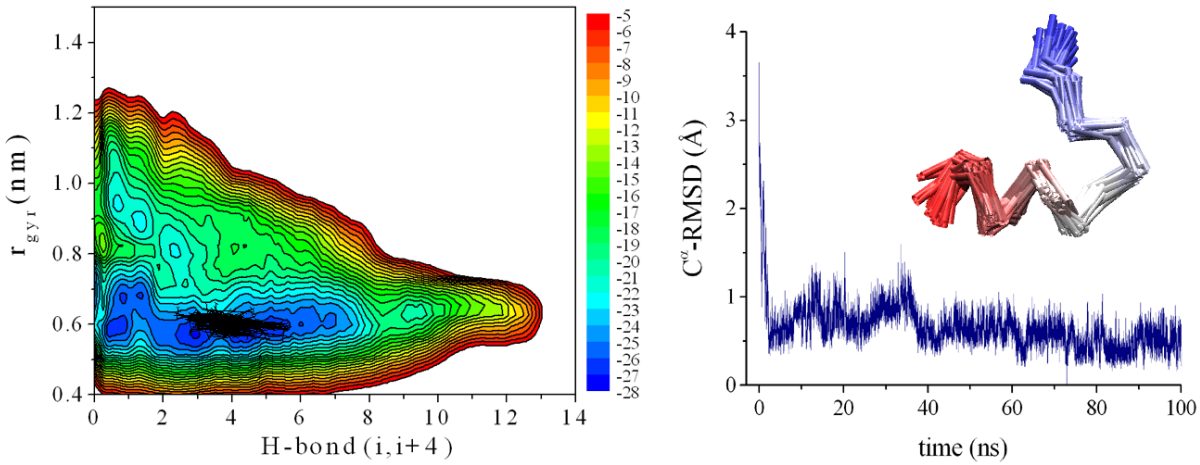

Figure S11. Standard MD simulations of 100ns merely sample basin b2 of the PT-MetaD. The MD has been carried out at 283 K by using the same force field and simulation parameters of the present PT-MetaD. (left) The background FES refers to that obtained by PT-MetaD; details of the plot are provided in the Figure 1 caption. The conformations explored by the 100 ns MD simulation are represented by a black line. (right) RMSD values calculated between the conformations sampled in the 100ns MD simulation and the median structure from the equilibrated part of this simulation. Intervaled conformations from the segment 10 ns – 100 ns are reported in the top of the right panel. The panel indicates that PrP-H1 undergoes a fast transition from the starting structure to the basin b2.